

Magnetism of $j=1/2$ moments on the fcc lattice in double perovskite Mott insulators

Ashley M. Cook¹, Stephanie Matern², Ciarán Hickey¹, Adam A. Aczel³, Arun Paramakanti^{1,4}

¹*Department of Physics, University of Toronto, Toronto, Ontario, Canada M5S 1A7*

²*Institute for Theoretical Physics, Cologne University, 50937 Cologne, Germany*

³*Quantum Condensed Matter Division, Oak Ridge National Lab, Oak Ridge, TN, 37831, USA and*

⁴*Canadian Institute for Advanced Research, Toronto, Ontario, M5G 1Z8, Canada*

Motivated by studies of Mott insulating double perovskites $\text{La}_2\text{ZnIrO}_6$ and $\text{La}_2\text{MgIrO}_6$, we consider magnetism of spin-orbit coupled $j = 1/2$ iridium moments on the geometrically frustrated face-centered cubic (fcc) lattice. Symmetry dictates that the nearest-neighbor exchange interaction includes, in addition to a Heisenberg term, compass-type and symmetric off-diagonal exchange couplings. Using a combination of Luttinger-Tisza and simulated annealing, we find a rich variety of magnetic phases, including collinear A-type antiferromagnetism as in $\text{La}_2\text{ZnIrO}_6$ and $\text{La}_2\text{MgIrO}_6$, collinear stripe order with moments along the $\{111\}/\{\bar{1}\bar{1}\bar{1}\}$ directions, and incommensurate non-coplanar multimode spirals. Using Monte Carlo simulations, we determine the magnetic transition temperature in these phases, and discuss experimental implications for $\text{La}_2\text{ZnIrO}_6$ and $\text{La}_2\text{MgIrO}_6$.

Introduction. — Heavy atoms with strong spin-orbit coupling (SOC) and electronic correlations are predicted to form exotic quantum phases [1]. Rare-earth ions on the frustrated pyrochlore lattice can lead to local moments with strong SOC which interact via unusual exchange couplings, leading to ‘quantum spin ice’ behavior as in $\text{Yb}_2\text{Ti}_2\text{O}_7$ [2–6]. Another exciting proposal is to realize the Kitaev Hamiltonian, with a spin liquid ground state and Majorana fermion excitations [7], in iridium oxides with edge-sharing octahedra, such as the two-dimensional (2D) honeycomb iridates Na_2IrO_3 and Li_2IrO_3 [8, 9]. Doping such Mott insulators has been predicted to lead to topological superconductivity [10]. Experimentally, in both Na_2IrO_3 and Li_2IrO_3 , the spin liquid state is preempted by magnetic order [11, 12] induced by exchange couplings beyond the Kitaev model. Nevertheless, extensive work on these materials [13–18], and the closely related 3D harmonic honeycomb iridates $\beta, \gamma\text{-Li}_2\text{IrO}_3$ [19–26], ascribes their magnetic orders to large Kitaev couplings or directional exchange interactions. Such exchange interactions may also occur in the triangular lattice iridate $\text{Ba}_3\text{IrTi}_2\text{O}_9$ [27].

In light of these studies, it is interesting to ask - how generic are these exotic exchange couplings in other frustrated 3D lattices? What kinds of phases do they support? Is there experimental evidence favoring such unusual interactions in other types of materials? Indeed, previous work has suggested that strong Kitaev-type interactions should be generically present in a large class of 2D and 3D iridates [28]. Here, we explore these issues in the context of ordered double perovskite (DP) compounds, a large class of materials with the chemical formula $\text{A}_2\text{BB}'\text{O}_6$, where B and B' ions occupy the two sublattices of a 3D cubic crystal. Metallic DPs such as $\text{Sr}_2\text{FeMoO}_6$ [29] have long been of interest as half-metallic ferromagnets [30–34]. Recent work on metallic DPs has examined the role of SOC on bulk spin dynamics [35], and topological states in ultrathin films [36–39]. On the other hand, DPs where B is an inert filled-shell

ion, and B' is a heavy $4d/5d$ ion, support Mott insulators with local moments on the frustrated fcc lattice of B' ions [40–48]. Our work is directly motivated by the recent synthesis of $\text{La}_2\text{ZnIrO}_6$ and $\text{La}_2\text{MgIrO}_6$ [49]. Structurally, $\text{La}_2\text{ZnIrO}_6$ and $\text{La}_2\text{MgIrO}_6$ have nearly undistorted oxygen octahedra. A nominal valence Ir^{4+} ($5d^5$), together with the strong SOC and larger spacing between Ir ions compared to perovskites, suggests that these materials behave as effective $j=1/2$ Mott insulators [49].

Below, we focus on the broad aspects of magnetism in an ideal fcc lattice, highlighting the rich physics of strong SOC in a canonical frustrated 3D lattice. Our main results are the following. (i) We show that even nearest-neighbor exchange interactions on the fcc lattice can lead to a rich variety of magnetic behaviors such as collinear antiferromagnets, stripes, or multimode spirals, due to the complex nature of symmetry-allowed couplings between spin-orbit coupled moments, which includes compass terms and symmetric off-diagonal exchange. (ii) We find that SOC can stabilize a regime of robust A-type antiferromagnetism (AFM), also called Type-I AFM, which is observed in neutron diffraction on $\text{La}_2\text{ZnIrO}_6$ and $\text{La}_2\text{MgIrO}_6$ [49]. (iii) In certain regimes with A-type AFM, we uncover a residual accidental degeneracy of collinear states. Quantum order by disorder is important in pinning moments along the Ir-O bond direction. This direction is consistent with *ab initio* results on $\text{La}_2\text{ZnIrO}_6$ and $\text{La}_2\text{MgIrO}_6$ [49]. (iv) Finally, we make contact with detailed experimental data on $\text{La}_2\text{ZnIrO}_6$ and $\text{La}_2\text{MgIrO}_6$ [49], arguing that they may host a large direction-dependent exchange interaction. A subtle variation in the magnetic ordering pattern between the two materials is shown to reconcile weak ferromagnetism in $\text{La}_2\text{ZnIrO}_6$ with its absence in $\text{La}_2\text{MgIrO}_6$.

Model. — To construct a minimal model on the fcc lattice of Ir moments, we consider the ideal cubic DP structure, and focus only on nearest neighbor terms which are expected to dominate. We appeal to symmetry arguments to write down all possible terms, based on the fact

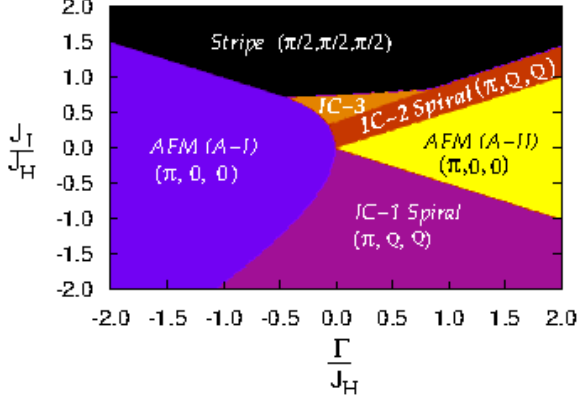


FIG. 1: Phase diagram of the spin Hamiltonian as a function of J_I/J_H vs Γ/J_H , obtained using the Luttinger-Tisza method, showing (i) A-type antiferromagnet A-I, having moments perpendicular to the ferromagnetic planes which are stacked antiferromagnetically, (ii) A-type antiferromagnet A-II having moments in the ferromagnetic planes which are stacked antiferromagnetically, (iii) Stripe order at $(\pi/2, \pi/2, \pi/2)$ with moments pointing in the $\{111\}/\{\bar{1}\bar{1}\bar{1}\}$ or symmetry related directions, and (iv) incommensurate spiral phases IC-1, IC-2, and IC-3. Beyond the Luttinger-Tisza analysis, the spirals are multimode states.

that the effective $j = 1/2$ angular momentum operator is a pseudovector (axial vector). Requiring invariance of the Hamiltonian under lattice rotational and mirror symmetries constrains the Hamiltonian coupling nearest-neighbor Ir sites to be of the form $H = H_H + H_I + H_{OD}$,

$$H_H = J_H \sum_{\langle \mathbf{r}\mathbf{r}' \rangle} \vec{S}_{\mathbf{r}} \cdot \vec{S}_{\mathbf{r}'} \quad (1)$$

$$H_I = J_I \left(\sum_{\langle \mathbf{r}\mathbf{r}' \rangle_{xy}} S_{\mathbf{r}}^z S_{\mathbf{r}'}^z + \sum_{\langle \mathbf{r}\mathbf{r}' \rangle_{yz}} S_{\mathbf{r}}^x S_{\mathbf{r}'}^x + \sum_{\langle \mathbf{r}\mathbf{r}' \rangle_{xz}} S_{\mathbf{r}}^y S_{\mathbf{r}'}^y \right) \quad (2)$$

$$H_{OD} = \Gamma \sum_{\mathbf{r}} \left[(S_{\mathbf{r}}^x S_{\mathbf{r}+x+y}^y + S_{\mathbf{r}}^y S_{\mathbf{r}+x+y}^x - S_{\mathbf{r}}^x S_{\mathbf{r}-x+y}^y - S_{\mathbf{r}}^y S_{\mathbf{r}-x+y}^x) + (x, y \leftrightarrow y, z) + (x, y \leftrightarrow x, z) \right] \quad (3)$$

Here, $\langle \mathbf{r}\mathbf{r}' \rangle$ denotes all nearest neighbor pairs, while $\langle \mathbf{r}\mathbf{r}' \rangle_{xy}$ denotes nearest neighbors restricted to the xy -plane (similarly for yz, xz). H_H is the Heisenberg term with exchange coupling J_I , H_I is an Ising-type term which yields compass anisotropy with strength J_I , and H_{OD} is a symmetric off-diagonal exchange term with coupling strength Γ . Antisymmetric Dzyaloshinskii-Moriya interactions are forbidden here by inversion symmetry.

Luttinger-Tisza analysis. — To determine the preferred magnetic orders, we use the Luttinger-Tisza method which considers the spins to be classical moments, and replaces the constant length spin vectors by unconstrained vector fields $\vec{\phi}_{\mathbf{r}}$. The classical spin Hamil-

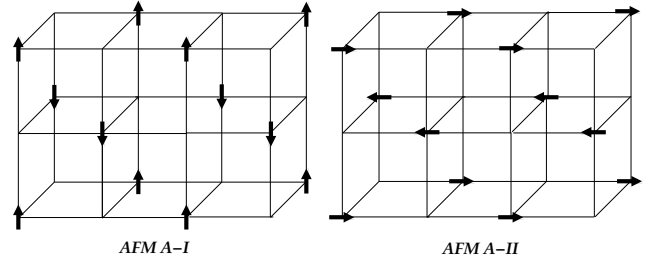


FIG. 2: Real space spin configurations in the layered A-type antiferromagnetic states AFM A-I and AFM A-II.

tonian written in momentum space then takes the form

$$H_{LT} = 2J_H \sum_{\mathbf{k}} \phi_{\mathbf{k}\mu}^* M_{\mu\nu}(\mathbf{k}) \phi_{\mathbf{k}\nu} \quad (4)$$

where the coupling matrix

$$M(\mathbf{k}) = \begin{pmatrix} A_{\mathbf{k}} + \alpha C_{\mathbf{k}}^{yz} & -\gamma S_{\mathbf{k}}^{xy} & -\gamma S_{\mathbf{k}}^{xz} \\ -\gamma S_{\mathbf{k}}^{xy} & A_{\mathbf{k}} + \alpha C_{\mathbf{k}}^{xz} & -\gamma S_{\mathbf{k}}^{yz} \\ -\gamma S_{\mathbf{k}}^{xz} & -\gamma S_{\mathbf{k}}^{yz} & A_{\mathbf{k}} + \alpha C_{\mathbf{k}}^{xy} \end{pmatrix} \quad (5)$$

with $A_{\mathbf{k}} = (\cos k_x \cos k_y + \cos k_x \cos k_z + \cos k_y \cos k_z)$, $C_{\mathbf{k}}^{ij} = \cos k_i \cos k_j$, and $S_{\mathbf{k}}^{ij} = \sin k_i \sin k_j$, and we have defined $\alpha = J_I/J_H$ and $\gamma = \Gamma/J_H$. Here, k_i (with $i = x, y, z$) denote components of the momentum along the cubic Ir-O axes, and we have set the Ir-O-M bond length ($M=\text{Zn, Mg}$) to unity. Diagonalizing H_{LT} , and looking for the lowest energy eigenvalue in \mathbf{k} , we find a rich variety of possible magnetically ordered phases as shown in Fig. 1.

Magnetic orders. — The Luttinger-Tisza analysis yields collinear as well as spiral antiferromagnetic states. We describe these phases below, and compare their energy with numerical simulated annealing results.

AFM A-I: This is an A-type collinear antiferromagnet (also referred to as a Type-I AFM in the literature) which consists of ferromagnetically ordered spins in the cubic ab -plane layered antiferromagnetically along the c -axis. The spins point along the c -axis, perpendicular to the ferromagnetic planes as shown in Fig. 2. There are six symmetry related A-I ground states, associated with a three-fold choice of the layering direction and a two-fold choice of the Ising antiferromagnetic order. Although these are the lowest energy collinear states, there is an accidental degeneracy in the classical limit where one can form multimode states leading to coplanar or even noncoplanar states with the same classical ground state energy. This degeneracy is expected to be broken in favor of collinear states by fluctuation effects, and our simulated annealing finds the above collinear states to be stabilized by thermal order by disorder.

AFM A-II: This is also an A-type collinear antiferromagnet; however the spins lie in the ferromagnetic planes as shown in Fig. 2. In addition to these collinear states, there are again multimode coplanar or noncoplanar states

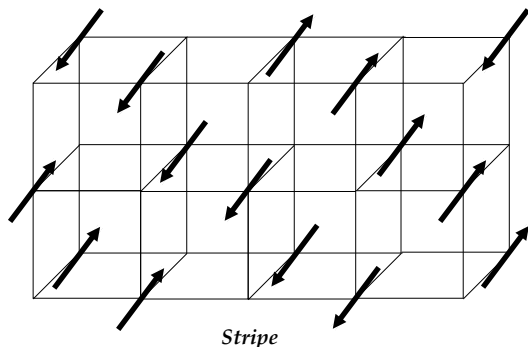


FIG. 3: Real space spin configurations in the collinear stripe state, showing moments pointing along the diagonal $\{111\}$ and $\{1\bar{1}\bar{1}\}$ directions for $(k_x, k_y, k_z) \equiv (\pi/2, \pi/2, \pi/2)$.

with the same classical ground state energy; again, we expect and observe numerically that thermal fluctuations favor the collinear orders over coplanar or noncoplanar orders. For the collinear order, the ground state energy is independent of the precise angle in the plane so that there is an accidental XY degeneracy of collinear states. We find that this degeneracy is broken by quantum fluctuations (see Supplemental Material), with the ‘order by disorder’ effect favoring spins along the Ir-O bond direction. Thermal fluctuations in the simulated annealing also favor the same collinear ordering. There are twelve symmetry related A-II ground states favored by fluctuations; these are associated with a three-fold choice of the layering direction and a four-fold choice of the spin axis.

Stripe: The collinear stripe state has moments pointing along the $\{111\}$ and $\{1\bar{1}\bar{1}\}$ directions arranged as shown in Fig. 3 for $(k_x, k_y, k_z) \equiv \pm(\pi/2, \pi/2, \pi/2)$; symmetry related orders are degenerate. Ordering with this wavevector is also referred to in the literature as a Type-II AFM. The ordering wavevector determines the direction of the spins, so that flipping one of the momentum components also flips the corresponding spin component; thus, ordering at $\pm(\pi/2, -\pi/2, \pi/2)$ leads to spins along $\{1\bar{1}1\}$ and $\{11\bar{1}\}$. This leads to a total of eight ground states.

Incommensurate Spiral (IC-1, IC-2): In these regimes, the Luttinger-Tisza analysis suggests an incommensurate coplanar spiral order with wavevector of the form $(k_x, k_y, k_z) \equiv (\pi, Q, Q)$, and symmetry related equivalents. With $\alpha = J_I/J_H$ and $\gamma = \Gamma/J_H$, minimizing the Luttinger-Tisza energy leads to $Q = \cos^{-1}(\frac{1+\alpha/2}{1+|\gamma|})$; the transition into the AFM A-I state ($Q = 0$) happens when $\alpha = 2|\gamma|$. However, we find that if we assume single mode ordering, the spins constructed in the IC-1 and IC-2 phases from the Luttinger-Tisza eigenvectors do not satisfy the constraint of constant magnitude. Using simulated annealing numerics, we find that the ground states in this regime are noncoplanar multimode spirals formed by superposing all six equivalent wavevectors $(\pi, Q, \pm Q)$, $(Q, \pi, \pm Q)$, $(Q, \pm Q, \pi)$.

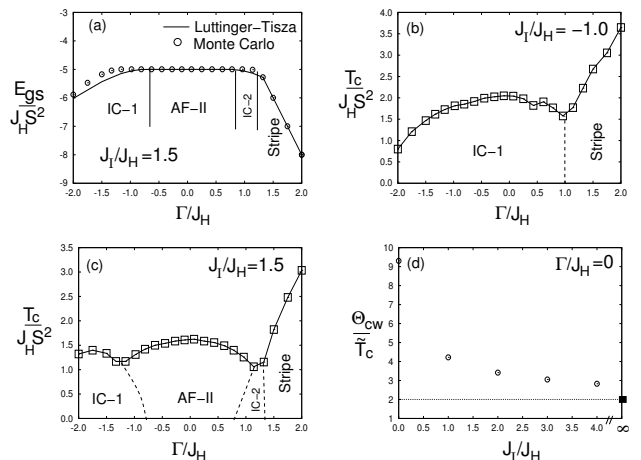


FIG. 4: (a): Comparison of the scaled ground state energy per spin E_{gs} obtained within Luttinger-Tisza method (solid line) and simulated annealing approach (dots). (b),(c): Magnetic transition temperature T_c of the classical model (in units of $J_H S^2$, for spin length S) vs. Γ/J_H , obtained using Monte Carlo simulations for cuts through the phase diagram (Fig. 1) at $J_I/J_H = -1.0, +1.5$. (d) Plot of the ‘frustration parameter’, the ratio of the magnetic transition temperature $\tilde{T}_c \equiv T_c(1 + 1/S)$ to the Curie-Weiss temperature Θ_{CW} ; here T_c is obtained using classical Monte Carlo simulations, and the rescaling by $(1 + 1/S)$ accounts for the classical S^2 being replaced by the quantum $S(S + 1)$. The dark square shows the result at $J_I/J_H \rightarrow \infty$.

Incommensurate Spiral (IC-3): In this regime, the Luttinger-Tisza approach again suggests an incommensurate coplanar spiral order; however, the wavevector is of the form $(k_x, k_y, k_z) \equiv (P, Q, Q)$. We have not found a simple closed form expression for P, Q ; however, they are obtained by minimizing the Luttinger-Tisza eigenvalue

$$\lambda = (4 + \alpha) \cos P \cos Q + (2 + \alpha) \cos^2 Q - \gamma \sin^2 Q - \sqrt{D} \quad (6)$$

$$D \equiv [\alpha(\cos P - \cos Q) \cos Q - \gamma \sin^2 Q]^2 + 8\gamma^2 \sin^2 P \sin^2 Q \quad (7)$$

Again, a single mode spiral does not satisfy the spin constraint, and our simulated annealing numerics again show noncoplanar multimode spiral order in this regime.

Monte Carlo results. — In order to confirm the magnetic orderings, we have used simulated annealing numerics to find the classical ground states. Fig. 4(a) compares the numerically computed ground state energy per spin to the Luttinger-Tisza result, for $J_I/J_H = 1.5$ and varying Γ/J_H . The agreement between the two is excellent in the AFM A-II and Stripe states, where the collinear order is precisely recovered within the Luttinger-Tisza approach. In the IC-1/IC-2 regimes, the simulated annealing approach, which preserves the spin constraint, indicates multimode order, and leads to an energy per spin (for 36^3 lattice) which is only slightly higher by $\lesssim 2\%$.

In order to determine the magnetic ordering temperature in the various phases, we have carried out Monte Carlo simulations on system sizes with up to 24^3 spins.

Fig. 4 shows the magnetic T_c as determined from the specific heat singularity, along various cuts through the Luttinger-Tisza phase diagram. The Heisenberg limit in the absence of SOC ($J_I = 0$, $\Gamma = 0$) is the most fragile state with the lowest $T_c \approx 0.44J_H S^2$; our results here agree with previous work on the fcc Heisenberg model [50], where thermal order by disorder leads to a nonzero T_c . The A-I and A-II phases and the stripe phase appear most robust with high T_c , since SOC enhances the pinning of the moment direction. Thus, although the exchange interactions induced by SOC are also frustrated on the fcc lattice, the SOC nevertheless enhances T_c by favoring certain spin orientations, thus reducing the effects of thermal disordering.

Comparison with experiments. — $\text{La}_2\text{ZnIrO}_6$ and $\text{La}_2\text{MgIrO}_6$ are DPs which order as A-type antiferromagnets. *Ab initio* studies [49] suggest that the Ir spins lie predominantly in the ferromagnetic planes (A-II state). Our work shows that this is consistent with $J_I > 0$ and $|\Gamma| < J_I/2$, and that quantum order-by-disorder is key to pinning moments along the Ir-O bond directions.

In the presence of anisotropic exchange interactions, the Curie-Weiss temperature of $j=1/2$ moments on the ideal fcc lattice is $\Theta_{CW} = -(3J_H + J_I)$, independent of Γ . However, both $\text{La}_2\text{ZnIrO}_6$ and $\text{La}_2\text{MgIrO}_6$ have a monoclinic $\text{P}2_1/n$ structure, arising from small octahedral rotations — an octahedral rotation ϕ about the cubic c -axis which is staggered between adjacent ab layers, and a global tilt about the cubic $\{110\}$ axis. We account for this within a simple approximation, in which strong SOC leads to moments which just track the octahedral rotation. This corresponds to making local rotations on the spins; within this approximation, the global tilts are innocuous, especially to interpret data on powder samples. This simple estimate ignores the renormalization of the exchange couplings caused by the rotation, which is expected to be unimportant for small rotation angles, and it provides a reasonable first understanding of magnetism in Sr_2IrO_4 [8, 51]. Using this approximation, a high temperature expansion yields a powder averaged $\Theta_{CW} = -J_H - \frac{1}{3}(2J_H + J_I)(1 + 2\cos 2\phi)$. At the same time, if the axis along which the ferromagnetic planes are stacked in staggered fashion coincides with the axis of the staggered octahedral rotations, there will be a net ferromagnetic moment $\approx m \sin \phi$ in the AFM A-II state, where m is the ordered moment. Finally, for small ϕ , we expect T_c to be only weakly renormalized; within the approximation of a unitary rotation it would be unchanged.

In $\text{La}_2\text{MgIrO}_6$, *ab initio* studies predict a ferromagnetic moment $\approx 0.3\mu_B$ based on the monoclinic $\text{P}2_1/n$ structure with staggered octahedral rotations; however, experiments do not detect any ferromagnetic moment in the ordered phase. To understand this discrepancy we propose that the axis of the staggered octahedral rotations and the stacking direction of the ferromagnetic planes are along orthogonal cubic axes, and *ab initio* re-

sults may have missed the correct ordering due to subtle energy differences between the different stackings. This can be tested if additional magnetic Bragg peaks in the neutron diffraction can be resolved. If we ignore SOC ($J_I = 0$, $\Gamma = 0$), and note that $\phi \approx 9^\circ$ from the structural data is small, the measured $\Theta_{CW} \approx -24K$ yields $J_H \approx 8K$. Our Monte Carlo simulations at $J_I = 0, \Gamma = 0$ show $T_c \approx 0.44J_H S^2$, consistent with previous work on the fcc Heisenberg model [50]. Heuristically replacing the classical S^2 by $S(S+1)$ for quantum spins leads to a renormalized $\tilde{T}_c = T_c(1 + 1/S)$, an approximation which works well for the 3D cubic lattice $S = 1/2$ Heisenberg model [52]. We find, with $J_H = 8K$ and $S = 1/2$, that $\tilde{T}_c \approx 2.6K$, much smaller than $T_c^{\text{expt}} = 12K$. Turning on $\Gamma \neq 0$, but keeping $J_I = 0$, hardly changes T_c or even suppresses T_c . This hints at a significant $J_I/J_H > 0$. Indeed, a plot of the “frustration parameter” $-\Theta_{CW}/\tilde{T}_c$, as shown in Fig. 4(d) for $\Gamma = 0$, illustrates that recovering the observed ratio $-\Theta_{CW}/\tilde{T}_c \approx 2$ needs a large directional exchange. Thus, we suggest that a model with only the J_I term, perturbed by a weak Heisenberg exchange coupling $J_H \ll J_I$ might be a suitable starting point to understand $j=1/2$ magnetism in $\text{La}_2\text{MgIrO}_6$; we estimate this dominant coupling $J_I \approx 24K$. These estimates do not shed much light on the off-diagonal symmetric exchange since the powder averaged Θ_{CW} is independent of Γ , and T_c is not very sensitive to Γ (see Fig. 4(c)). However $|\Gamma| > \alpha/2$ is precluded by the observed order.

In $\text{La}_2\text{ZnIrO}_6$, there is a measured ferromagnetic moment $\approx 0.22\mu_B$; thus, the axis along which the ferromagnetic planes are stacked in staggered fashion must coincide with the axis of the staggered octahedral rotations. If we set $\phi \approx 11^\circ$, to be consistent with structural data, we expect a moment $\approx 0.19\mu_B$, close to the measured value. This is smaller than the *ab initio* prediction $\approx 0.5\mu_B$. Based on the smaller $T_c^{\text{expt}} \approx 7.5K$ in $\text{La}_2\text{ZnIrO}_6$, and assuming similar ratios of exchanges, $J_H/J_I \ll 1$, we estimate the dominant $J_I \approx 15K$, and $\Theta_{CW} \approx -15K$; however, experiments report $\Theta_{CW} \approx -3K$ [49]. The origin of this discrepancy remains to be clarified.

In summary, we have shown that double perovskite Mott insulators provide a remarkable class of materials which host unusual and strongly direction-dependent exchange interactions. Our study also motivates a search for DPs with large Γ , which might lead to spiral order, or stripes with moments along the $\{111\}$ direction. Further work is needed to derive the exchange Hamiltonian from a microscopic viewpoint, explore possible exotic spin liquids which might be stabilized by such interactions on the fcc lattice, and variants of DP Mott insulators with magnetic ions on both B and B' sublattices [53].

We thank G. Chen, J. P. Clancy, B. D. Gaulin, J. E. Greedan, Y. J. Kim, and S. Trebst for useful discussions. We acknowledge funding from NSERC of Canada. S.M. was supported by the Bonn-Cologne Graduate School of Physics and Astronomy.

-
- [1] W. Witczak-Krempa, G. Chen, Y. B. Kim, and L. Balents, *Ann. Rev. of Cond. Matt. Phys.* **5**, 57 (2014).
- [2] K. A. Ross, L. Savary, B. D. Gaulin, and L. Balents, *Phys. Rev. X* **1**, 021002 (2011).
- [3] S. Lee, S. Onoda, and L. Balents, *Phys. Rev. B* **86**, 104412 (2012).
- [4] O. Benton, O. Sikora, and N. Shannon, *Phys. Rev. B* **86**, 075154 (2012).
- [5] Y. Wan and O. Tchernyshyov, *Phys. Rev. Lett.* **108**, 247210 (2012).
- [6] L. Pan, S. K. Kim, A. Ghosh, C. M. Morris, K. A. Ross, E. Kermarrec, B. D. Gaulin, S. M. Koohpayeh, O. Tchernyshyov, and N. P. Armitage, *Nat Commun* **5** (2014).
- [7] A. Kitaev, *Annals of Physics* **321**, 2 (2006).
- [8] G. Jackeli and G. Khaliullin, *Phys. Rev. Lett.* **102**, 017205 (2009).
- [9] J. Chaloupka, G. Jackeli, and G. Khaliullin, *Phys. Rev. Lett.* **105**, 027204 (2010).
- [10] Y.-Z. You, I. Kimchi, and A. Vishwanath, *Phys. Rev. B* **86**, 085145 (2012).
- [11] X. Liu, T. Berlijn, W.-G. Yin, W. Ku, A. Tsvelik, Y.-J. Kim, H. Gretarsson, Y. Singh, P. Gegenwart, and J. P. Hill, *Phys. Rev. B* **83**, 220403 (2011).
- [12] S. K. Choi, R. Coldea, A. N. Kolmogorov, T. Lancaster, I. I. Mazin, S. J. Blundell, P. G. Radaelli, Y. Singh, P. Gegenwart, K. R. Choi, et al., *Phys. Rev. Lett.* **108**, 127204 (2012).
- [13] Y. Singh, S. Manni, J. Reuther, T. Berlijn, R. Thomale, W. Ku, S. Trebst, and P. Gegenwart, *Phys. Rev. Lett.* **108**, 127203 (2012).
- [14] V. M. Katukuri, S. Nishimoto, V. Yushankhai, A. Stoyanova, H. Kandpal, S. Choi, R. Coldea, I. Rousochatzakis, L. Hozoi, and J. van den Brink, *New Journal of Physics* **16**, 013056 (2014).
- [15] J. G. Rau, E. K.-H. Lee, and H.-Y. Kee, *Phys. Rev. Lett.* **112**, 077204 (2014).
- [16] J. G. Rau and H.-Y. Kee, *ArXiv e-prints* (2014), 1408.4811.
- [17] J. Reuther, R. Thomale, and S. Rachel, *Phys. Rev. B* **90**, 100405 (2014).
- [18] Y. Szyzuk, C. Price, P. Wölfle, and N. B. Perkins, *Phys. Rev. B* **90**, 155126 (2014).
- [19] T. Takayama, A. Kato, R. Dinnebier, J. Nuss, and H. Takagi, *ArXiv e-prints* (2014), 1403.3296.
- [20] K. A. Modic, T. E. Smidt, I. Kimchi, N. P. Breznay, A. Biffin, S. Choi, R. D. Johnson, R. Coldea, P. Watkins-Curry, G. T. McCandless, et al., *Nat Commun* **5** (2014).
- [21] A. Biffin, R. D. Johnson, I. Kimchi, R. Morris, A. Bombardi, J. G. Analytis, A. Vishwanath, and R. Coldea, *Phys. Rev. Lett.* **113**, 197201 (2014).
- [22] I. Kimchi, R. Coldea, and A. Vishwanath, *ArXiv e-prints* (2014), 1408.3640.
- [23] E. K.-H. Lee, R. Schaffer, S. Bhattacharjee, and Y. B. Kim, *Phys. Rev. B* **89**, 045117 (2014).
- [24] S. Lee, E. K.-H. Lee, A. Paramakanti, and Y. B. Kim, *Phys. Rev. B* **89**, 014424 (2014).
- [25] E. Kin-Ho Lee and Y. B. Kim, *ArXiv e-prints* (2014), 1407.4125.
- [26] H.-S. Kim, E. Kin-Ho Lee, and Y. B. Kim, *ArXiv e-prints* (2015), 1502.00006.
- [27] M. Becker, M. Hermanns, B. Bauer, M. Garst, and S. Trebst, *ArXiv e-prints* (2014), 1409.6972.
- [28] I. Kimchi and A. Vishwanath, *Phys. Rev. B* **89**, 014414 (2014).
- [29] K. I. Kobayashi, T. Kimura, H. Sawada, K. Terakura, and Y. Tokura, *Nature (London)* **395** (1998).
- [30] D. D. Sarma, P. Mahadevan, T. Saha-Dasgupta, S. Ray, and A. Kumar, *Phys. Rev. Lett.* **85**, 2549 (2000).
- [31] T. Saha-Dasgupta and D. D. Sarma, *Phys. Rev. B* **64**, 064408 (2001).
- [32] L. Brey, M. J. Calderón, S. Das Sarma, and F. Guinea, *Phys. Rev. B* **74**, 094429 (2006).
- [33] L. Alff, in *Electron Correlation in New Materials and Nanosystems*, Vol. **241** of NATO Science Series, edited by K. Sharnberg and S. Kruchinin (Springer, Netherlands) (2007).
- [34] O. Erten, O. N. Meetei, A. Mukherjee, M. Randeria, N. Trivedi, and P. Woodward, *Phys. Rev. Lett.* **107**, 257201 (2011).
- [35] K. W. Plumb, A. M. Cook, J. P. Clancy, A. I. Kolesnikov, B. C. Jeon, T. W. Noh, A. Paramakanti, and Y.-J. Kim, *Phys. Rev. B* **87**, 184412 (2013).
- [36] A. Cook and A. Paramakanti, *Phys. Rev. B* **88**, 235102 (2013).
- [37] A. M. Cook and A. Paramakanti, *Phys. Rev. Lett.* **113**, 077203 (2014).
- [38] A. M. Cook, C. Hickey, and A. Paramakanti, *Phys. Rev. B* **90**, 085145 (2014).
- [39] H. Zhang, H. Huang, K. Haule, and D. Vanderbilt, *Phys. Rev. B* **90**, 165143 (2014).
- [40] T. Aharen, J. E. Greedan, C. A. Bridges, A. A. Aczel, J. Rodriguez, G. MacDougall, G. M. Luke, V. K. Michaelis, S. Kroecker, C. R. Wiebe, et al., *Phys. Rev. B* **81**, 064436 (2010).
- [41] T. Aharen, J. E. Greedan, C. A. Bridges, A. A. Aczel, J. Rodriguez, G. MacDougall, G. M. Luke, T. Imai, V. K. Michaelis, S. Kroecker, et al., *Phys. Rev. B* **81**, 224409 (2010).
- [42] M. A. de Vries, A. C. Mclaughlin, and J.-W. G. Bos, *Phys. Rev. Lett.* **104**, 177202 (2010).
- [43] A. J. Steele, P. J. Baker, T. Lancaster, F. L. Pratt, I. Franke, S. Ghannadzadeh, P. A. Goddard, W. Hayes, D. Prabhakaran, and S. J. Blundell, *Phys. Rev. B* **84**, 144416 (2011).
- [44] A. A. Aczel, D. E. Bugaris, L. Li, J.-Q. Yan, C. de la Cruz, H.-C. zur Loye, and S. E. Nagler, *Phys. Rev. B* **87**, 014435 (2013).
- [45] G. Chen, R. Pereira, and L. Balents, *Phys. Rev. B* **82**, 174440 (2010).
- [46] T. Dodds, T.-P. Choy, and Y. B. Kim, *Phys. Rev. B* **84**, 104439 (2011).
- [47] G. Chen and L. Balents, *Phys. Rev. B* **84**, 094420 (2011).
- [48] H. Ishizuka and L. Balents, *Phys. Rev. B* **90**, 184422 (2014).
- [49] G. Cao, A. Subedi, S. Calder, J.-Q. Yan, J. Yi, Z. Gai, L. Poudel, D. J. Singh, M. D. Lumsden, A. D. Christianson, et al., *Phys. Rev. B* **87**, 155136 (2013).
- [50] H. T. Diep and H. Kawamura, *Phys. Rev. B* **40**, 7019 (1989).
- [51] F. Wang and T. Senthil, *Phys. Rev. Lett.* **106**, 136402 (2011).
- [52] A. W. Sandvik, *Phys. Rev. Lett.* **80**, 5196 (1998).
- [53] O. N. Meetei, O. Erten, M. Randeria, N. Trivedi, and P. Woodward, *Phys. Rev. Lett.* **110**, 087203 (2013).

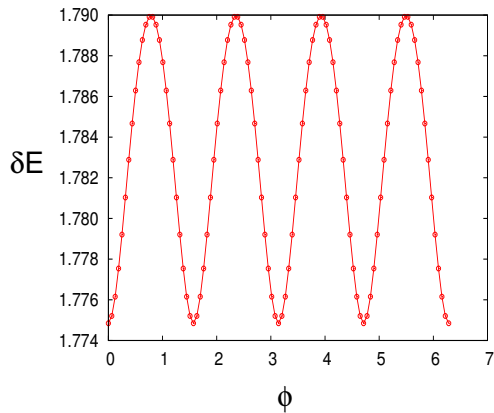


FIG. 5: Plot of the ϕ -dependent zero point energy contribution δE (in units of J_H) at $J_I/J_H = 1, \Gamma = 0$, showing minima at discrete values of $\phi = n\pi/2$ ($n = 0, 1, 2, 3$). Similar results follow at $\Gamma \neq 0$ and other values of J_I/J_H in the A-II phase.

Quantum order by disorder

Assuming that the spins in the AFM A-II state lie in the cubic xy plane, and make an angle ϕ with the x -axis,

the classical ground state energy is independent of ϕ . We evaluate the contribution from zero point fluctuations using a standard Holstein-Primakoff spin wave expansion. For simplicity, we quote the explicit result at $\Gamma = 0$, but qualitatively similar results hold for nonzero Γ . At $\Gamma = 0$, the spin wave energy $\Omega_{\mathbf{k}}(\phi) = \sqrt{(P_{\mathbf{k}} + R_{\mathbf{k}})^2 - F_{\mathbf{k}}^2}$, where

$$P_{\mathbf{k}} = 2(J_H + J_I) + C_{\mathbf{k}}^{xy}(2J_H + J_I) \quad (8)$$

$$R_{\mathbf{k}} = J_I(C_{\mathbf{k}}^{xz} \cos^2\phi + C_{\mathbf{k}}^{yz} \sin^2\phi) \quad (9)$$

$$F_{\mathbf{k}} = J_I(-C_{\mathbf{k}}^{xy} + C_{\mathbf{k}}^{xz} \cos^2\phi + C_{\mathbf{k}}^{yz} \sin^2\phi) + 2J_H(C_{\mathbf{k}}^{xz} + C_{\mathbf{k}}^{yz}) \quad (10)$$

leading to a ϕ -dependent zero point energy contribution per site $\delta E = \frac{1}{2} \int_{\mathbf{k}} \Omega_{\mathbf{k}}(\phi)$. Here, we have defined $C_{\mathbf{k}}^{ij} = \cos k_i \cos k_j$ as in the main text of the paper. We plot δE in Fig. 5, showing that it has discrete minima at $\phi = n\pi/2$ ($n = 0, 1, 2, 3$). Quantum fluctuations in the presence of SOC thus break the accidental classical degeneracy in ϕ , favoring spins to point along the Ir-O bond directions in the ferromagnetic plane. Classical thermal fluctuations also favor the same directions as confirmed from our Monte Carlo simulations.